THE JOURNAL OF PHYSICAL CHEMISTRY A

Article

pubs.acs.org/JPCA

Impact of Sub-Doppler Measurements on Centrifugal-Distortion Terms: Rotational Spectrum of Methyl Fluoride Revisited

Gabriele Cazzoli and Cristina Puzzarini*

Dipartimento di Chimica "Giacomo Ciamician", Università di Bologna, Via F. Selmi 2, 40126 Bologna, Italy

Supporting Information

ABSTRACT: Methyl fluoride is a prototypical symmetric-top molecule. Despite the fact that its rotational spectrum has been largely investigated, centrifugal-distortion constants were determined only up to the sextic terms. The present investigation demonstrates the importance of sub-Doppler measurements in the terahertz region not only for deriving higher-order centrifugal-distortion terms but also for revising the parameters available in the literature. The Lamb-dip technique has been exploited for obtaining sub-Doppler resolution in the 102 GHz to 1.2 THz frequency range, thus allowing for the improvement of all spectroscopic parameters. Furthermore, the hyperfine structure due to fluorine and hydrogens has been resolved, thus enabling the determination of the corresponding spin−rotation constants with an accuracy rivaling that obtained by molecular-beam electric resonance measurements and of the dipolar spin−spin coupling constants for the first time. The prediction and analysis of hyperfine structures were guided and supported by high-level quantum-chemical calculations of the parameters involved.

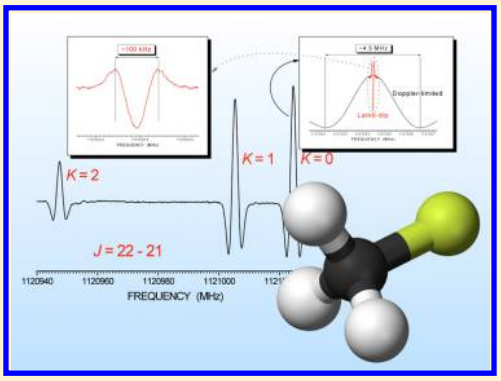

INTRODUCTION

Although the key role played by rotational spectroscopy in atmospheric and astrophysical studies has been well-known for decades,[1] rather new is its extension to the terahertz domain with precision, accuracy, and sensitivity comparable to those obtainable in the millimeter-/submillimeter-wave regions.[2−7] The proliferation and increased abilities of remote-sensing missions for monitoring planetary atmospheres and of astronomical telescopes for space observations have spurred the need for the knowledge of either accurate transition frequencies in the terahertz regime or their derivation based on accurate spectroscopic parameters. The last point is the topic touched upon by the present work.

Though methyl fluoride (CH_3F) is of interest only to Earth's atmosphere studies, the reinvestigation of its rotational spectrum allowed us to point out the importance of accurate measurements, at sub-Doppler resolution, on the derivation of the centrifugal-distortion terms of the effective rotational Hamiltonian. The accurate and reliable determination of the latter parameters is a key point in the extrapolation from laboratory measurements to higher frequencies. In this respect, CH_3F has been chosen because of the limited characterization of its rotational spectrum. Despite being a molecule of interest for both experimental and theoretical spectroscopy (see ref 8 and references therein), prior to this work, its rotational parameters were known only up to the sextic terms and, from the beginning of our investigation, it was clear that they were required to be extended, improved, and in some cases revised. Furthermore, methyl fluoride is a prototypical prolate symmetric-top molecule and its potential energy surface has recently been the subject of investigations aiming at a complete vibro-rotational characterization.[8−10] Nikitin et al.[8] and Manson et al.[9,10] pointed out the challenge of an accurate theoretical description of its vibrational energy levels and of the proper account of vibrational polyads and resonance couplings.

CH_3F was also chosen because of its intrinsic interest. For example, reactions involving methyl fluoride have attracted attention because of the important roles played in atmospheric and combustion chemistry (see, for example, refs 11−13 and references therein). Because the fluorinated methanes, namely CF_4 (Freon 14), CHF_3 (Freon 23), CH_2F_2 (Freon 32), and CH_3F (freon 41), are environmentally less harmful than the fully halogenated chloro-fluorocarbons (CFCs), they were suggested as their replacements.[14] Their main impact on the environment is therefore related with global warming. On one end, CH_3F has a low global warming potential and is no longer in use today. On the other end, the atmospheric CH_4 mixing ratio has increased because of anthropogenic sources and methyl fluoride has been found to be an effective inhibitor of methane oxidation and production (see ref 15 and references therein). To understand the impact of anthropogenic activities on the environment, climate models have been developed. Most of them account for the chemical processes taking place in the atmosphere and therefore require a precise knowledge of the thermodynamic and

Special Issue: 25th Austin Symposium on Molecular Structure and Dynamics

Received: August 21, 2014
Revised: November 12, 2014
Published: November 12, 2014

dx.doi.org/10.1021/jp508459q | J. Phys. Chem. A 2015, 119, 1765−1773

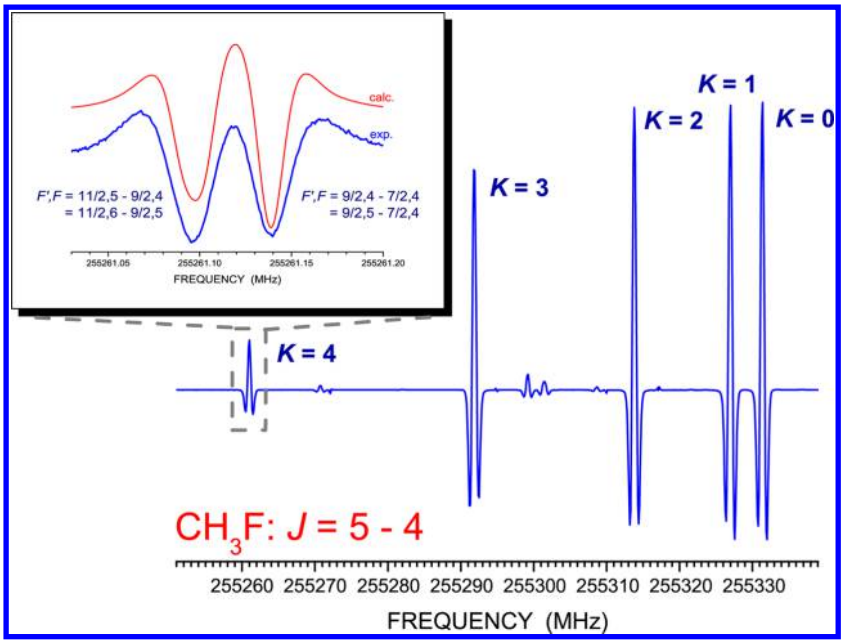

Figure 1. K structure (with $K = 0-4$) of the $J = 5 \leftarrow 4$ rotational transition recorded at $P = 2$ mTorr (modulation depth = 300 kHz). In the inset, the hyperfine structure of the $K = 4$ component is shown in detail (recorded at $P = 0.5$ mTorr, modulation depth = 15 kHz).

kinetic properties of the atmospheric reactions involved.[16] This need led, for example, to the recent investigation of the thermochemistry of atmospherically important halomethane derivatives, also including CH_3F, by means of high-precision quantum-chemical calculations.[17]

The last comments concern the most recent studies of the rotational spectrum of methyl fluoride,[18,19] because some measurements will be used in the present work and they report the parameters we aim at improving. In ref 18, the submillimeter-wave spectrum of CH_3F up to 1.625 THz was observed with transition frequencies retrieved in most cases with an uncertainty of 500 kHz. These measurements allowed for the first "accurate" determination of the sextic constants. Subsequently, Papousek et al.[19] recorded the far-infrared spectrum of CH_3F with an accuracy of 1.5 MHz up to ~3 THz. These data were simultaneously fit with previous rotational and vibro-rotational measurements, thus enabling the revision of the sextic terms of ref 18. The consideration of vibrorotational transitions allowed them to also determine the A_0 and D_K constants.[19] As will be demonstrated later in the text, the spectroscopic parameters of ref 19 turned out to be insufficiently accurate to reproduce our sub-Doppler measurements. Because the Lamb-dip technique presented here allowed us to resolve the hyperfine structure due to fluorine and hydrogens, the work by Wofsy, Muenter, and Klemperer[20] should also be mentioned. In that study, the authors measured the molecular-beam electric resonance spectrum of methyl fluoride in several rotational states, and from the analysis of the hyperfine structures they determined the corresponding parameters, namely, the spin−rotation constants, of both fluorine and hydrogens. On the other hand, they did not account for the dipolar spin−spin parameters, which have been derived for the first time in the present study.

In passing, we mention the infrared-terahertz double-resonance spectroscopy of methyl fluoride and methyl chloride at atmospheric pressure: in ref 5 a spectroscopic tool for highly selective remote sensing of atmospheric trace polar molecular gases is presented.

EXPERIMENTAL DETAILS

Measurements were performed with a frequency-modulated computer-controlled spectrometer working from 65 GHz to 1.6 THz,[21,22] with the 102 GHz to 1.58 THz frequency range actually considered. The Lamb-dip technique[23,24] was employed to obtain sub-Doppler resolution[25,26] and was applied in the 102 GHz to 1.2 THz frequency range. Doppler-limited measurements were carried out using a free-space cell with a single-path arrangement, whereas the double-path configuration as well as a terahertz Fabry−Perot interferometer, constructed using suitable metallic meshes, were employed in the Lamb-dip measurements (for details, the reader is referred to ref 25). Doppler-limited measurements were performed in the 1.5−1.6 THz range and for very weak transitions at frequencies below 1.2 THz.

Our spectrometer is a modification[22,25] of the terahertz spectrometer described in detail refs 21 and 27. The millimeter- and submillimeter-wave sources employed, phase-locked to a rubidium frequency standard, were either frequency multipliers driven by Gunn diode oscillators or Gunn diode oscillators themselves. The frequency modulation was obtained by sine-wave modulating the 72 MHz local oscillator of the synchronization loop. For Doppler-limited measurements, the modulation depth was varied from 100 kHz to 3.0 MHz, according to the transition frequency under consideration. For the Lamb-dip recordings, modulation-depth values ranging from 4 to 72 kHz were used. Liquid-He cooled InSb detector was used, with Schottky diode detectors also employed at frequencies below 500 GHz. In both cases, the output was processed by means of a Lock-in amplifier tuned to twice the modulation frequency, and thus performing second harmonic detection.

With respect to the experimental conditions, a commercial sample (purity >99%) was used without further purification. Doppler-limited measurements were carried out at pressure values ranging from 0.3 to 50 mTorr. For Lamb-dip measurements, low pressure values (0.1−1.2 mTorr) were chosen to minimize the dip widths as much as possible and to avoid frequency shifts.

dx.doi.org/10.1021/jp508459q | J. Phys. Chem. A 2015, 119, 1765−1773

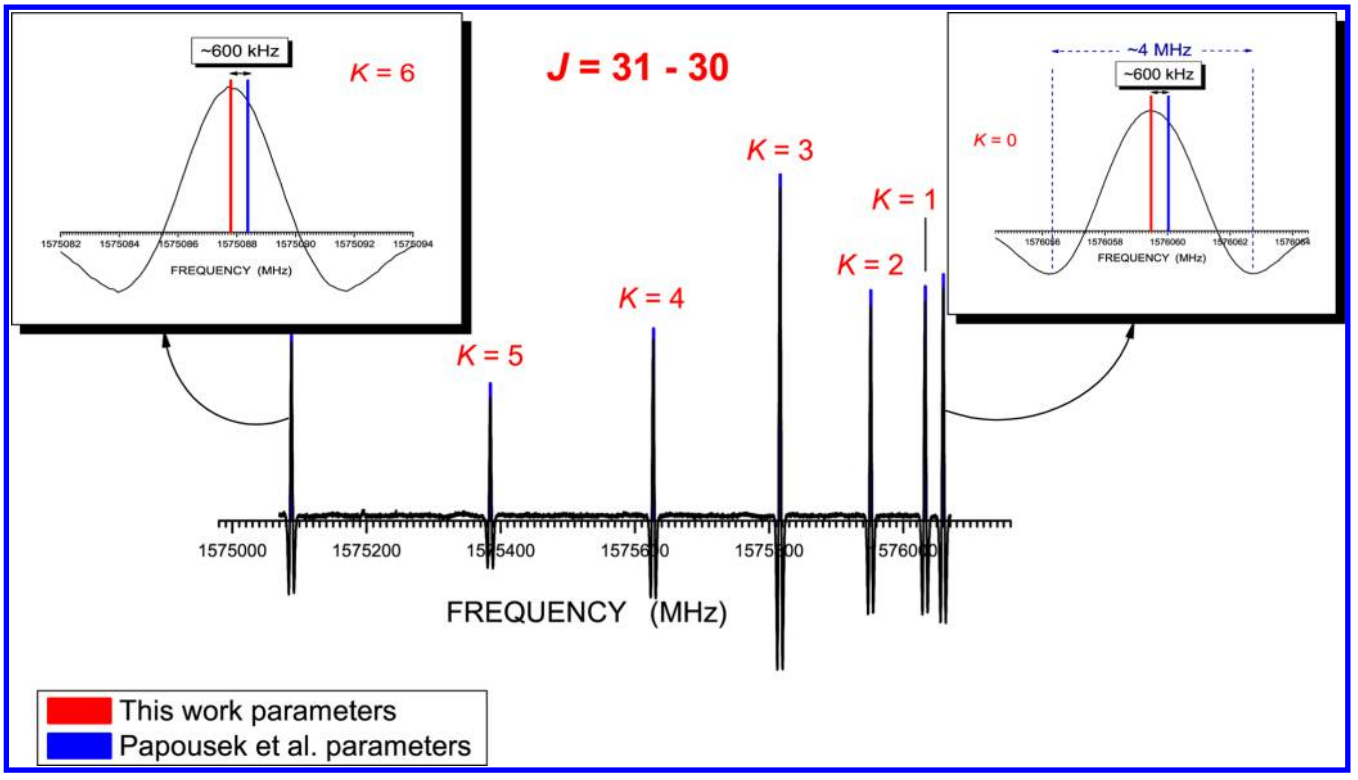

Figure 2. K structure (with $K = 0–6$) of the $J = 31 \leftarrow 30$ rotational transition recorded at $P = 2$ mTorr (modulation depth = 3 MHz). In the insets, the Doppler-limited recordings of the $K = 0$ and 6 components ($P = 2$ mTorr, modulation depth = 1.8 MHz) are shown together with the corresponding predictions based on this work and on the parameters of ref 19.

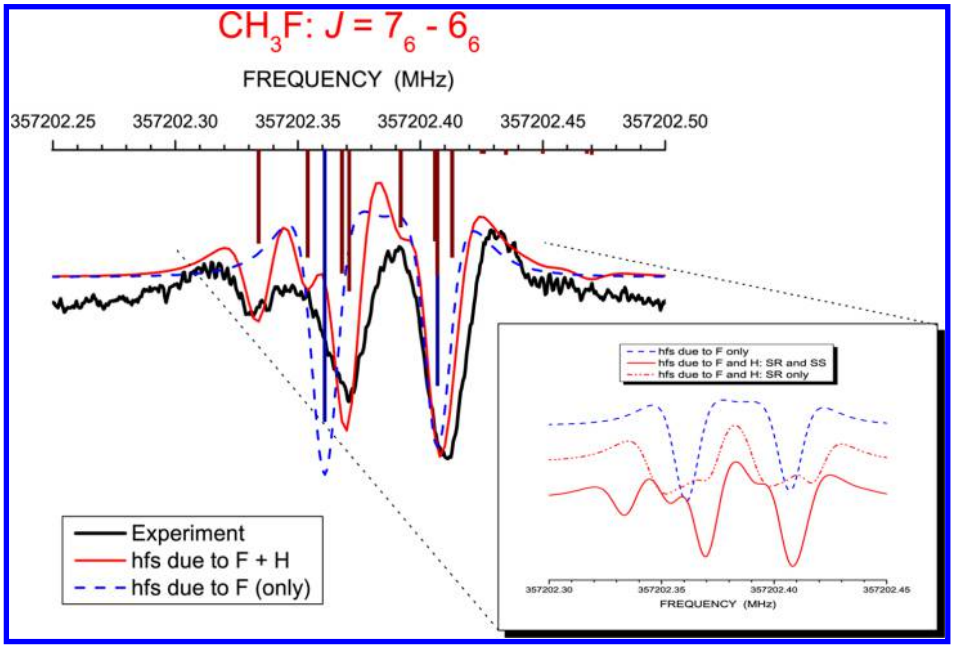

Figure 3. Hyperfine structure (hfs) of the $K = 6$ component of the $J = 7 \leftarrow 6$ rotational transition recorded using the Lamb-dip technique ($P = 0.4$ mTorr, modulation depth = 10.5 kHz). Simulated and stick spectra based on computed hyperfine parameters are also shown to point out how hfs modifies by consideration of fluorine only (in blue) to the additional inclusion of hydrogens (in red). In the inset, the simulated hfs is depicted with consideration of fluorine only (dashed blue line), with consideration of fluorine and hydrogen spin–rotation constants (SR; dash-dot-dot red line), and also with inclusion of dipolar spin–spin coupling constants (SS; solid red line).

SPECTRAL ANALYSIS

Figures 1 and 2 depict the characteristic K structure of the $J = 5 \leftarrow 4$ and $J = 31 \leftarrow 30$ rotational transitions, respectively. Figure 2 makes it evident that the $K = 3n$ lines are expected to be more intense than the other ones due to the hydrogen nuclear-spin statistics. It is also worth noting the very good signal-to-noise ratio (S/N) of the observed spectra, even in the 1.57 THz region. Figure 1 shows in the inset the Lamb-dip recording of the $K = 4$ transition; the doublet observed is essentially due to the fluorine

dx.doi.org/10.1021/jp508459q | J. Phys. Chem. A 2015, 119, 1765–1773

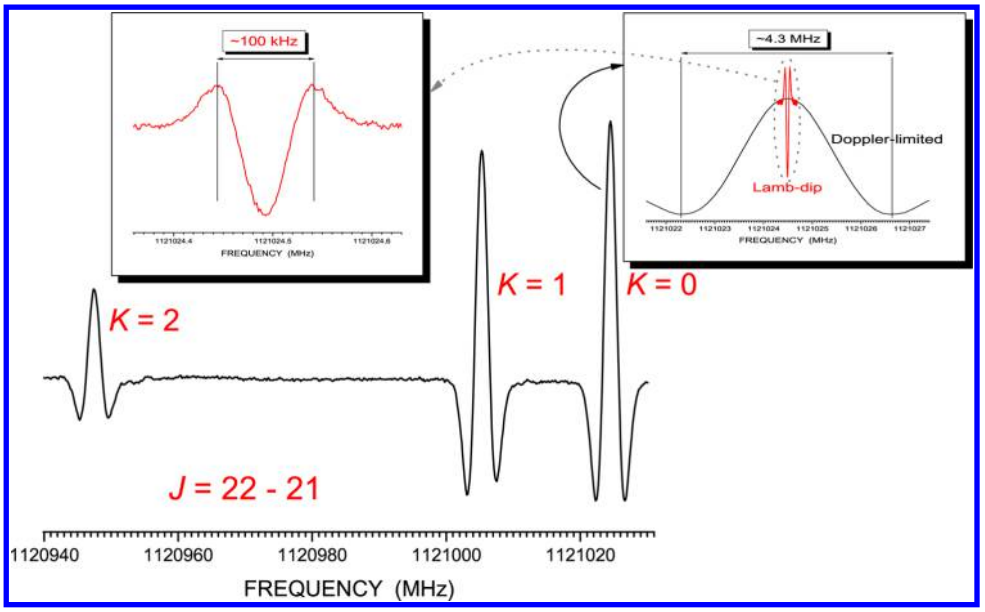

Figure 4. K structure (with $K = 0-2$) of the $J = 22 \leftarrow 21$ rotational transition recorded at $P = 0.3$ mTorr (modulation depth = 1.35 MHz). In the inset on the right is shown the overlap of the Lamb-dip ($P = 0.4$ mTorr, modulation depth = 45 kHz) and Doppler-limited recordings of the $K = 0$ component; the full line width for the latter case is pointed out. In the inset on the left, the Lamb-dip spectrum is better shown together with the corresponding full line width.

spin−rotation interaction, with the hydrogen spin−rotation and dipolar spin−spin interactions only leading to a broadening of the observed features. The hyperfine structure shown in the inset of Figure 1 is rather representative of that shown in most of the recorded Lamb-dip spectra. In fact, the splitting due to the spin−rotation interaction increases by enlarging the value of K, but actually only for a few $K = 3$ and 6 transitions could we observe a different hyperfine structure. Though the effective Hamiltonian used for the analysis is introduced below, we here note that Figure 3 provides an example of how the hyperfine structure evolves from the consideration of fluorine only to the inclusion of spin rotation for hydrogens and then of the dipolar spin−spin coupling terms. Hyperfine structures could be resolved up to 611 GHz; Lamb-dip measurements at higher frequencies only permitted us to retrieve very accurate transition frequencies.

The hyperfine components result from the ΔF_1, $\Delta F = +1$, 0, −1 selection rules, where F_1 and F are the hyperfine quantum numbers coming from the coupling schemes $F_1 = J + I_F$ and $F = F_1 + I_{tot}$, where I_F is the nuclear spin of fluorine and I_{tot} is the sum of the nuclear spins of the three H nuclei.

The effective Hamiltonian can be written as

$$\mathbf{H} = \mathbf{H}_{ROT} + \mathbf{H}_{SR} + \mathbf{H}_{SS} \quad (1)$$

where $\mathbf{H}_{ROT}$ is the rotational Hamiltonian operator for a symmetric-top molecule,[28] including centrifugal-distortion terms up to the octics.

$$\mathbf{H}_{SR} = \sum_{K} \mathbf{I}_L \cdot \mathbf{C}_K \cdot \mathbf{J} \quad (2)$$

is the spin−rotation Hamiltonian[29,30] written in terms of a second-rank tensor $\mathbf{C}_L$ coupled with the rotational and nuclear-spin momenta. The sum runs over all L nuclei of the molecule having nonzero nuclear spin (i.e., all atoms but carbon in the present case). Finally, $\mathbf{H}_{SS}$ is the dipolar spin−spin Hamiltonian[29,30]

$$\mathbf{H}_{SS}^{(LM)} = \mathbf{I}_L \mathbf{D}^{LM} \mathbf{I}_M \quad (3)$$

with L and M denoting either H and F or H and H. The relevant dipolar spin−spin terms are D_1, D_2, and D_3, which correspond to 0.5 times the D_{zz} (H−F) component changed in sign, to the half difference of the D_{yy} and D_{xx} components $[(D_{yy} - D_{xx})/2]$ of the H−F spin−spin tensor, and to the D_{zz} component of the H−H dipolar spin−spin coupling tensor, respectively (for the expressions of D_1, D_2, and D_3, the reader is for example referred to refs 31 and 32).

For predicting the hyperfine pattern of the rotational spectra, we made use of the spin−rotation and spin−spin constants determined by quantum-chemical calculations, as explained in the following section. Simulations based on computed hyperfine parameters (as exemplified by the inset of Figure 3) allowed us to identify those transitions that show hyperfine structures with a sizable effect due to hydrogens.

To accurately retrieve the transition frequencies from the recorded spectra, for the distorted and/or partially blended features, we resorted to a line-profile analysis[33,34] using the Lorentzian function and the Voigt profile model for Lamb-dip and Doppler-limited measurements, respectively. In all the other cases, the experimental data points were fit with a parabolic function.[a] However, in all cases the frequency values were obtained as averages of sets of measurements. On the basis of the standard deviations of these averages, the transition intensities and the S/N,[35,36] we estimated the experimental uncertainties to range from 10 to 20 kHz for Doppler-limited measurements and to conservatively be 1 kHz for the Lamb-dip ones (with only a few exceptions due to the low S/N). Figure 4, which depicts the $K = 0$ to $K = 2$ components of the $J = 22 \leftarrow 21$ rotational transition, demonstrates how the full line width is reduced when going from Doppler-limited to Lamb-dip measurements (from about 4.3 MHz to ∼100 kHz). Therefore, Figure 4 makes it evident that also in the terahertz frequency range, transition frequencies can be retrieved with an accuracy of 1 kHz by exploiting the Lamb-dip technique.

dx.doi.org/10.1021/jp508459q | J. Phys. Chem. A 2015, 119, 1765−1773

Table 1. Ground-State Spectroscopic Parameters for $^{12}CH_3F$

parameter		this work: exp: only our meas[a]	this work: exp: global fit[b]	this work: theo[c]	Papousek et al.[19]	Wosfy et al.[20]
A_0	MHz	[155352.56][d]	[155352.56][d]	155124.26	155352.56(68)	
B_0	MHz	25536.149656(16)	25536.149648(12)	25536.49	25536.14755(26)	
D_J	kHz	60.228435(89)	60.228359(47)	58.30	60.21744(60)	
D_{JK}	kHz	439.61315(38)	439.61325(34)	436.41	439.5708(92)	
D_K	kHz	*d*	*d*	2083.83	2106.923(1.930)	
H_J	mHz	−26.91(16)	−27.087(67)	−21.93	−31.241(139)	
H_{JK}	Hz	1.81462(49)	1.81474(46)	1.71	1.8058(29)	
H_{KJ}	Hz	21.9563(29)	21.9572(26)	20.57	21.4096(479)	
H_K	kHz	*d*	*d*	85.47		
L_J	Hz	−0.559(95)	−0.432(23)			
L_{JJK}	mHz					
L_{JK}	mHz	−0.0540(24)	−0.0552(22)			
L_{KKJ}	mHz	−1.4516(93)	−1.4509(87)			
C_N(F)	kHz	−4.50(58)	−4.44(55)	−4.38		−4.0(1.9)
C_K(F)	kHz	55.7(12)	55.8(11)	51.37		51.1(1.3)
$(C_{xx} + C_{yy})(H)/2$	kHz	[−0.47]	[−0.47]	−0.47		−0.8(1.5)
C_{zz}(H)	kHz	−11.9(11)	−12.0(10)	−14.57		−14.66(70)
D_1(F−H)	kHz	10.8(25)	10.7(23)	8.16		
D_2(H−H)	kHz	[5.42]	[5.42]	5.42		
D_3(F−H)	kHz	24.5(22)	24.5(21)	20.28		
$\overline{\chi}^{e}$		0.95	0.91			

[a]Values in brackets were kept fixed in the fitting procedure: A_0 to Papousek et al.[19] value, hyperfine parameters to computed values. Only our measurements were considered. Standard errors (as derived from the SPFIT output using Kisiel's PIFORM code[60]) in the least significant digit(s) are given in parentheses. [b]Values in brackets were kept fixed in the fitting procedure: A_0 to Papousek et al.[19] value, hyperfine parameters to computed values. All available measurements from the literature were included in the fit.[18,19,25] See text. Standard errors (as derived from the SPFIT output using Kisiel's PIFORM code[60]) in the least significant digit(s) are given in parentheses. [c]Equilibrium rotational constants as straightforwardly derived from the equilibrium structure of ref 43. Equilibrium values of the hyperfine parameters at the CCSD(T)/cc-pCV5Z level, with all electrons correlated and using the equilibrium structure of ref 43. Vibrational corrections to hyperfine parameters and quartic and sextic centrifugal-distortion constants at the CCSD(T)/cc-pCVTZ level, with all electrons correlated. See text. [d]Parameters nondeterminable by fitting only pure rotational transitions.[28] [e]Dimensionless (weighted) standard deviation.

QUANTUM-CHEMICAL CALCULATIONS

Quantum-chemical calculations of the rotational, centrifugal-distortion, and hyperfine constants were carried out with the CFOUR program package.[37] An exhaustive account on this topic can be found in refs 38 and 39, where the theoretical background and computational procedures are described in detail, but in the following we provide a brief summary of the relevant points.

To achieve the accuracy required for a quantitative prediction of the experiment, calculations were performed using the coupled-cluster singles and doubles (CCSD) method augmented by a perturbative treatment of triple excitations (CCSD(T))[40] in conjunction with the cc-pCV5Z basis set,[41,42] with all electrons being correlated. Equilibrium parameters were computed at the semiexperimental equilibrium structure derived by Demaison et al.[43] The vibrational corrections to hyperfine parameters and rotational constants as well as the quartic and sextic centrifugal-distortion constants were evaluated by means of second-order vibrational perturbation theory (VPT2)[44] at the CCSD(T)/cc-pCVTZ level (with all electrons correlated).

The ground-state rotational constants were derived by augmenting the equilibrium rotational constants B_e^i (straightforwardly derived from the semiexperimental equilibrium structure[43]) for vibrational corrections ΔB_0^i:[44]

$$B_0^{\mathrm{i}} = B_{\mathrm{e}}^{\mathrm{i}} + \Delta B_0^{\mathrm{i}} = B_{\mathrm{e}}^{\mathrm{i}} - \frac{1}{2}\sum_r \alpha_r^{\mathrm{i}} \quad (4)$$

where the α_r^i's are the vibration−rotation interaction constants, with the sum running over all normal modes and i denoting the inertial axis.

As concerns the spin−rotation interaction, each element of the spin−rotation tensor has an electronic and a nuclear contribution. As implemented in CFOUR, the electronic contribution was evaluated as the second derivative of the electronic energy with respect to the rotational angular momentum and the nuclear spin $\mathbf{I}_L$[45−47] in conjunction with perturbation-dependent basis functions (usually referred to as rotational London atomic orbitals[45]). The nuclear contribution only depends on the geometrical structure of the molecule. The expression for the components of the dipolar spin−spin coupling tensor $\mathbf{D}^{LM}$ can be found, for instance, in refs 28, 48, and 49. They only depend on molecular structure, thus not requiring any electronic structure calculation. Quantum chemistry was employed for computing the vibrational corrections to the equilibrium values.

Vibrational corrections to both spin−rotation and dipolar spin−spin constants were obtained as the difference between the vibrationally averaged and equilibrium values. As implemented in CFOUR, vibrational averaging of properties is accomplished via an expansion of the expectation value over the vibrational-wave function in a Taylor series around the equilibrium value with respect to the normal-coordinate displacements.[50] The cubic force field required for the vibrational averaging and for the evaluation of the vibration−rotation interaction and centrifugal-distortion constants, was obtained by computing the harmonic

dx.doi.org/10.1021/jp508459q | J. Phys. Chem. A 2015, 119, 1765−1773

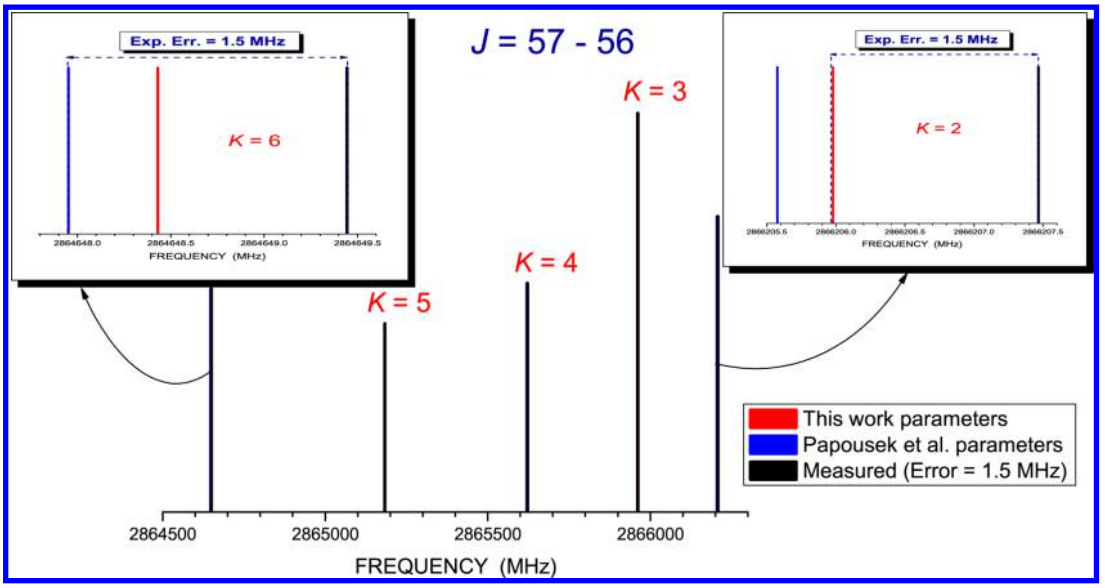

Figure 5. Schematic representation of the K structure (with $K = 2-6$) of the $J = 57 \leftarrow 56$ rotational transition. The measured frequency values (in black) are compared with the corresponding predictions based on this work (in red) and ref 19 (in blue) parameters. In the insets, this comparison is made evident and the experimental uncertainty is also reported.

part in a fully analytic manner,[51,52] and the cubic force constants as well as the corresponding derivatives of the considered property using finite-difference techniques.[52,53]

RESULTS AND DISCUSSION

A total of 230 distinct frequency lines were measured in the 102 GHz to 1.6 THz frequency range. The frequency values are provided in the Supporting Information, together with the fit output. The new measurements were independently fit and were included in global fit involving all previous pure rotational frequency (or wavenumber) values available up to approximately 3 THz for the vibrational ground state.[18,19,25] The fits were carried out using Pickett's SPFIT program,[54,55] with each transition weighted proportionally to the inverse square of its experimental uncertainty. The obtained spectroscopic parameters are collected in Table 1 where they are compared with those by Papousek et al.,[19] which provides the most recent and accurate previous results for CH_3F, and to the hyperfine parameters by Wosfy et al.[20] Quantum-chemical results are also reported.

From Table 1 it is evident that the present measurements allowed us to improve the uncertainties in the rotational and quartic centrifugal-distortion constants by 1 order of magnitude. The situation is different for the sextic centrifugal-distortion terms, because an important revision that deserves to be discussed in detail has been obtained. On the one hand, we note that the fit involving only our transitions is able to already well determine the sextics and 3 octic centrifugal-distortion terms. On the other hand, the inclusion of transition frequencies up to 3 THz permits us to improve the determination of H_J and L_J by reducing the corresponding uncertainties by more than 2 times and by about 4 times, respectively. For H_{JK} and H_{KJ}, the present results are larger than those of ref 19 by about 0.5% (i.e., ~4 times the standard error given in ref 19) and 2.5% (i.e., ~10 times the standard error given in ref 19), respectively. For H_J, the present work leads to a rather different value, the latter differing by about 23 times the standard error given in ref 19. These large discrepancies are not due to the inclusion of the octic centrifugal-distortion terms in the set of determinable parameters; in fact, a global fit without their inclusion leads to values very similar to those collected in the second column of Table 1, with the corresponding fit affected by a large standard deviation ($\overline{\chi^2} = 7.8$). The discrepancy pointed out mostly derives by the inclusion of sub-Doppler measurements in the terahertz region. The improvement provided by our investigation is already evident at 1.57 THz and it is exemplified by Figure 2, which shows the recording at a Doppler-limited resolution of the $J = 31 \leftarrow 30$, with $K = 0-6$, rotational transition: a systematic deviation of ~600 kHz of the line positions based on the parameters of ref 19 is observed. On the other hand, it has to be noted that the frequency values of ref 19 are usually affected by an uncertainty of 1.5 MHz. Therefore, a more significant example is provided by Figure 5, which depicts the comparison of the predictions based on our spectroscopic parameters and those based on the constants of ref 19 with the actual measurements[19] for the $J = 57 \leftarrow 56$, with $K = 2-6$, rotational transition at 2.86 THz. It is evident that our predictions better reproduce the experimental data, with those based on the spectroscopic parameters of ref 19 sometimes lying outside the error interval. The overall conclusion of the discussion above is the importance of accurate measurements, possibly at a sub-Doppler resolution, to accurately and reliably determine centrifugal-distortion terms, which in turn are required for the accurate prediction of higher frequency values.

As concerns quantum-chemical results, we note that the experimental rotational constants are reproduced with an accuracy of about 0.1% or better, and centrifugal-distortion constants show discrepancies of a few percent. H_J is the parameter showing the largest deviation, ~19%, but it has to be noted that H_J is about 3 orders of magnitude smaller than the other sextics. On the contrary, the computed value of H_K is expected to be affected by an error of about 5–6%, thus providing the first reliable determination for this constant.

In Table 1, the hyperfine parameters determined in the present work are compared with the computed ones and those obtained by molecular-beam electric resonance spectroscopy.[20] For what concerns fluorine, it is noted not only that C_N compares well with the theoretical and previous experimental data but also that we improved its accuracy by reducing the uncertainty by about 4

dx.doi.org/10.1021/jp508459q | J. Phys. Chem. A 2015, 119, 1765–1773

times. Different is the situation for C_K, for which our standard error is similar to that of ref 20, but with the corresponding value deviating from latter by about 4 times the standard deviation. Our high-level quantum-chemical calculations tends to confirm the determination of ref 20. A similar situation is observed for the C_{zz} component of the hydrogen spin−rotation tensor (with z corresponding to the a inertial axis), but with the discrepancy reduced to about 2 times the standard error. The effect of hydrogens on the hyperfine structure is exemplified in Figure 3, which shows the hyperfine structure of the $K = 6$ component of the $J = 7 \leftarrow 6$ rotational transition. In addition to the recorded spectrum, simulations based on the computed hyperfine parameters are depicted. In detail, it is shown how the hyperfine structure modifies from the consideration of fluorine only to the inclusion of the spin−rotation interaction for hydrogens and the subsequent account for the dipolar spin−spin coupling. It is evident that the hyperfine structure observed is explained only once all the possible interactions are taken into account. For this reason, we could also determine in addition to C_{zz} (H), the D_1 and D_3 constants, though with uncertainties of about 20% and 10%, respectively. These large errors are essentially due to the incomplete resolutions of the hyperfine features. Because the agreement with the computed values is within 1−2 times the standard error, the obtained values can be considered reliable. Because our computed hyperfine parameters were used to judge the reliability of experimental results, their accuracy should be pointed out. According to the literature on this topic (see, for examples, refs 56−59), the level of theory used is expected to provide values already converged with respect to the basis set extension and the wave function model. Subsequent inclusion of vibrational corrections then leads to the determination of hyperfine parameters accurate within 1 kHz.[38,39,56−59]

CONCLUDING REMARKS

In the present work, it has been demonstrated that Lamb-dip measurements in the terahertz region have a strong impact on the determination of accurate and reliable centrifugal-distortion constants. Despite the availability of transition frequencies up to 3 THz,[19] the inclusion of our accurate measurements could lead to the improvement and revision of the sextic centrifugal-distortion terms. Different fits have been carried out to assess the effect of these sub-Doppler measurements. It has to be noted that lowering their weight in the fit (i.e., by increasing the assigned uncertainties) systematically decreases the accuracy of the determined constants. Once an uncertainty of a few hundred kilohertz is assigned, the octic terms become barely determinable.

In conclusion, our sub-Doppler measurements, carried out in the 102 GHz to 1.2 THz range, allowed us to improve the rotational and quartic and sextic centrifugal-distortion constants and to determine three octics for the first time. Lamb-dip measurements also permitted us to resolve the hyperfine structure due to fluorine and hydrogens, thus enabling the derivation of spin−rotation constants with an accuracy comparable to that obtainable by molecular-beam electric resonance measurements and the determination of two dipolar spin−spin coupling constants for the first time. In the prediction and analysis of the hyperfine structures, a key role was played by high-level quantum-chemical calculations of the parameters involved.

ASSOCIATED CONTENT

Supporting Information

Output of Pickett's SPFIT program containing the list of measured frequencies together with the corresponding fit residuals (observed − calculated differences) and spectroscopic parameters. This material is available free of charge via the Internet at http://pubs.acs.org

AUTHOR INFORMATION

Corresponding Author

*C. Puzzarini. E-mail: cristina.puzzarini@unibo.it.

Notes

The authors declare no competing financial interest.

ACKNOWLEDGMENTS

This work has been supported by MIUR ("PRIN 2012" funds - project "STAR: Spectroscopic and computational Techniques for Astrophysical and atmospheric Research") and by the University of Bologna (RFO funds).

ADDITIONAL NOTE

[a]As routinely done in rotational spectroscopy and as implemented in many software packages for high-resolution spectroscopy, our software package for spectral display and analysis permits the baseline subtraction (if required) and the interpolation of the top of the line with the suitable parabolic function, i.e., with the parabola that accurately reproduces the top of the line.

REFERENCES

(1) Winnewisser, G.; Herbst, E.; Ungerechts, H. Spectroscopy Among the Stars. In *Spectroscopy of the Earth's Atmosphere and Interstellar Medium*; Rao, K. N., Weber, A., Eds.; Academic Press: San Diego, CA, 1992; pp 423−518.

(2) Drouin, B. J. Rotational Spectroscopy at the Jet Propulsion Laboratory. In *Remote Sensing of the Atmosphere for Environmental Security*; Perrin, A., Ben Sari-Zizi, N., Demaison, J., Eds.; NATO ARW series; Springer: Dordrecht, The Netherlands, 2006; pp257−269.

(3) Drouin, B. J.; Yu, S.; Pearson, J. C.; Gupta, H. Terahertz Spectroscopy for Space Applications: 2.5−2.7 THz Spectra of HD, H_2O and NH_3. *J. Mol. Struct.* **2012**, *1006*, 2−12.

(4) De Lucia, F. C. The Submillimeter: A Spectroscopist's View. *J. Mol. Spectrosc.* **2010**, *261*, 1−17.

(5) Phillips, D. J.; Tanner, E. A.; De Lucia, F. C.; Everitt, H. O. Infrared-Terahertz Double-Resonance Spectroscopy of CH_3F and CH_3Cl at Atmospheric Pressure. *Phys. Rev. A* **2012**, *85*, 052507/1−13.

(6) Brünken, S.; Müller, H. S. P.; Endres, C.; Lewen, F.; Giesen, T.; Drouin, B.; Pearson, J. C.; Mäder, H. High Resolution Rotational Spectroscopy on D_2O up to 2.7 THz in Its Ground and First Excited Vibrational Bending States. *Phys. Chem. Chem. Phys.* **2007**, *9*, 2103−2112.

(7) Cazzoli, G.; Cludi, L.; Buffa, G.; Puzzarini, C. Precise THz Measurements of HCO^+, N_2H^+, and CF^+ for Astrophysical Observations. *Astrophys. J. Suppl. S.* **2012**, *203*, 11/1−9.

(8) Nikitin, A. V.; Rey, M.; Tyuterev, V. G. Rotational and Vibrational Energy Levels of Methyl Fluoride Calculated from a New Potential Energy Surface. *J. Mol. Spectrosc.* **2012**, *274*, 28−34.

(9) Manson, S. A.; Law, M. M. General Internal Coordinate Gradient Vectors and the Vibrational Kinetic Energy Operator of Centrally-Connected Penta-Atomic Systems. Part I. *Phys. Chem. Chem. Phys.* **2006**, *8*, 2848−2854.

(10) Manson, S. A.; Law, M. M.; Atkinson, I. A.; Thomson, G. A. The Molecular Potential Energy Surface and Vibrational Energy Levels of Methyl Fluoride. Part II. *Phys. Chem. Chem. Phys.* **2006**, *8*, 2855−2865.

(11) Shu, J.; Lin, J. J.; Lee, Y. T.; Yang, X. Multiple Channel Dynamics of the O+CH_3F Reaction. *J. Chem. Phys.* **2000**, *113*, 9678−9685.
(12) Angel, L. A.; Garcia, S. P.; Ervin, K. M. Dynamics of the Gas-Phase Reactions of Chloride Ion with Fluoromethane: High Excess Translational Activation Energy for an Endothermic S_{N2} Reaction. *J. Am. Chem. Soc.* **2002**, *124*, 336−345.
(13) Yu, F.; Wu, L.; Liu, S.; Zhou, X. Static and Dynamic Reaction Pathways Involved in the Reaction of O^- and CH_3F. *J.Mol. Struct. THEOCHEM* **2010**, *947*, 1−8.
(14) Molina, M. J.; Rowland, F. S. Stratospheric Sink for Chlorofluoromethanes: Chlorine Atom-Catalysed Destruction of Ozone. *Nature* **1974**, *249*, 810−812.
(15) Frenzel, P.; Bosse, U. Methyl Fluoride, an Inhibitor of Methane Oxidation and Methane Production. *FEMS Microbiol. Ecol.* **1996**, *21*, 25−36.
(16) Nohende Ajavon, A.-L.; Albritton, D. L.; Watson, R. T. *Scientific Assessment of Ozone Depletion: 2006; Global Ozone Research Monitoring Project, Report No. 50*; World Meteorological Organization: Geneva, Switzerland, 2007.
(17) Csontos, J.; Rolik, Z.; Das, S.; Kállay, M. High-Accuracy Thermochemistry of Atmospherically Important Fluorinated and Chlorinated Methane Derivatives. *J. Phys. Chem. A* **2010**, *114*, 13093−13103.
(18) Brown, F. X.; Dangoisse, D.; Gadhi, J.; Wlodarczak, G.; Demaison, J. Millimeter-Wave and Submillimeter-Wave Spescroscopy of Methyl Fluoride. *J. Mol. Struct.* **1988**, *190*, 401−407.
(19) Papousek, D.; Hsu, Y.-C.; Chen, H. S.; Pracna, P.; Klee, S.; Winnewisser, M.; Demaison, J. Far Infrared Spectrum and Ground State Parameters of $^{12}CH_3F$. *J. Mol. Spectrosc.* **1993**, *159*, 33−41.
(20) Wofsy, S. C.; Muenter, J. S.; Klemperer, W. Determination of Hyperfine Constants and Nuclear Shielding in Methyl Fluoride and Comparison with Other Molecules. *J. Chem. Phys.* **1971**, *55*, 2014−2019.
(21) Cazzoli, G.; Puzzarini, C. The Lamb-Dip Spectrum of Methylcyanide: Precise Rotational Transition Frequencies and Improved Ground-State Rotational Parameters. *J. Mol. Spectrosc.* **2006**, *240*, 153−163.
(22) Puzzarini, C.; Cazzoli, G.; Gauss, J. The Rotational Spectra of $HD^{17}O$ and $D_2{}^{17}O$: Experiment and Quantum-Chemical Calculations. *J. Chem. Phys.* **2012**, *137*, 154311/1−10.
(23) Costain, C. C. The Use of Saturation Dip Absorption in Microwave Spectroscopy and in Microwave Frequency Stabilization. *Can. J. Phys.* **1969**, *47*, 2431−2433.
(24) Winton, R. S.; Gordy, W. High Precision Millimeter-Wave Spectroscopy with the Lamb Dip. *Phys. Lett. A* **1979**, *32*, 219−220.
(25) Cazzoli, G.; Puzzarini, C. Sub-Doppler Resolution in the THz Frequency Domain: 1 kHz Accuracy at 1 THz by Exploiting the Lamb-Dip Technique. *J. Phys. Chem. A* **2013**, *117*, 13759−13766.
(26) Cazzoli, G.; Dore, L. Observation of Crossing Resonances in the Hyperfine Structure of the J = 1 - 0 Transition of $DC^{15}N$. *J. Mol. Spectrosc.* **1990**, *143*, 231−236.
(27) Cazzoli, G.; Puzzarini, C.; Buffa, G.; Tarrini, O. Pressure-Broadening in the THz Frequency Region: the 1.113 THz Line of Water. *J. Quant. Spectrosc. Radiat. Transfer* **2008**, *109*, 1563−1574.
(28) Gordy, W.; Cook, R. L. In *Microwave Molecular Spectra*, 3rd ed.; Weissberger, A., Ed.; Wiley: New York, 1984.
(29) Townes, C. H.; Schawlow, A. L. *Microwave Spectroscpy*; McGraw-Hill: New York, 1955.
(30) Flygare, W. H. Magnetic Interactions in Molecules and an Analysis of Molecular Electronic Charge Distribution from Magnetic Parameters. *Chem. Rev.* **1974**, *74*, 653−687.
(31) Gunther-Mohr, G. R.; Townes, C. H.; Van-Vleck, J. H. Hyperfine Structure in the Spectrum of $^{14}NH_3$. II. Theoretical Discussion. *Phys. Rev.* **1954**, *94*, 1191−1203.
(32) Oddershede, J.; Paidarova, I.; Spirko, V. The Vibrational Dependence of the Magnetic Hyperfine Interaction Constants of Ammonia. *J. Mol. Spectrosc.* **1992**, *152*, 342−354.
(33) Cazzoli, G.; Dore, L. Lineshape Measurements of Rotational Lines in the Millimeter-Wave Region by Second Harmonic Detection. *J. Mol. Spectrosc.* **1990**, *141*, 49−58.
(34) Dore, L. Using Fast Fourier Transform to Compute the Line Shape of Frequency-Modulated Spectral Profiles. *J. Mol. Spectrosc.* **2003**, *221*, 93−98.
(35) Cazzoli, G.; Puzzarini, C.; Lapinov, A. V. Precise Laboratory Frequencies for the J ← J - 1 (J = 1, 2, 3, 4) Rotational Transitions of ^{13}CO. *Astrophys. J.* **2004**, *611*, 615−620.
(36) Landman, D. A.; Roussel-Dupré, R.; Tanigawa, G. On the Statistical Uncertainties Associated with Line Profile Fitting. *Astrophys. J.* **1982**, *261*, 732−735.
(37) Stanton, J. F.; Gauss, J.; Harding, M. E.; Szalay, P. G. CFOUR A Quantum Chemical Program Package. 2011; with contributions from Auer, A. A.; Bartlett, R. J.; Benedikt, U.; et al. and the integral packages MOLECULE (Almlöf, J.; Taylor, P. R.), PROPS (Taylor, P. R.), ABACUS (Helgaker, T. H.; et al.), and ECP routines by Mitin, A. V.; van Wüllen, C. For the current version, see http://www.cfour.de.
(38) Puzzarini, C.; Stanton, J. F.; Gauss, J. Quantum-Chemical Calculation of Spectroscopic Parameters for Rotational Spectroscopy. *Int. Rev. Phys. Chem.* **2010**, *29*, 273−367.
(39) Puzzarini, C. Rotational Spectroscopy Meets Theory. *Phys. Chem. Chem. Phys.* **2013**, *15*, 6595−6607.
(40) Raghavachari, K.; Trucks, G. W.; Pople, J. A.; Head-Gordon, M. A Fifth-Order Perturbation Comparison of Electron Correlation Theories. *Chem. Phys. Lett.* **1989**, *157*, 479−483.
(41) Dunning, T. H., Jr. Gaussian Basis Sets for Use in Correlated Molecular Calculations. I. The Atoms Boron Through Neon and Hydrogen. *J. Chem. Phys.* **1989**, *90*, 1007−1023.
(42) Woon, D. E.; Dunning, T. H., Jr. Gaussian Basis Sets for Use in Correlated Molecular Calculations. V. Core-Valence Basis Sets for Boron Through Neon. *J. Chem. Phys.* **1995**, *103*, 4572−4585.
(43) Demaison, J.; Breidung, J.; Thiel, W.; Papousek, D. The Equilibrium Structure of Methyl Fluoride. *Struct. Chem.* **1999**, *10*, 129−133.
(44) Mills, I. M. In *Molecular Spectroscopy: Modern Research*; Rao,K. N., Mathews, C. W., Eds.; Academic Press: New York, 1972.
(45) Gauss, J.; Ruud, K.; Helgaker, T. Perturbation-Dependent Atomic Orbitals for the Calculation of Spin-Rotation Constants and Rotational g Tensors. *J. Chem. Phys.* **1996**, *105*, 2804−2812.
(46) Gauss, J.; Stanton, J. F. Perturbative Treatment of Triple Excitations in Coupled-Cluster Calculations of Nuclear Magnetic Shielding Constants. *J. Chem. Phys.* **1996**, *104*, 2574−2583.
(47) Gauss, J.; Sundholm, D. Coupled-Cluster Calculations of Spin-Rotation Constants. *Mol. Phys.* **1997**, *91*, 449−458.
(48) Abragam, A. *Principles of Nuclear Magnetism*; Oxford University Press: New York, 1961.
(49) Schmidt-Rohr, K.; Spiess, H. W. *Multidimensional Solid State NMR and Polymers*; Academic Press: New York, 1994.
(50) Auer, A. A.; Gauss, J.; Stanton, J. F. Quantitative Prediction of Gas-Phase ^{13}C Nuclear Magnetic Shielding Constants. *J. Chem. Phys.* **2003**, *118*, 10407−10417.
(51) Gauss, J.; Stanton, J. F. Analytic CCSD(T) Second Derivatives. *Chem. Phys. Lett.* **1997**, *276*, 70−77.
(52) Stanton, J. F.; Gauss, J. Analytic Second Derivatives in High-Order Many-Body Perturbation and Coupled-Cluster Theories: Computational Considerations and Applications. *Int. Rev. Phys. Chem.* **2000**, *19*, 61−96.
(53) Stanton, J. F.; Lopreore, C. L.; Gauss, J. The Equilibrium Structureand Fundamental Vibrational Frequencies of Dioxirane. *J. Chem. Phys.* **1998**, *108*, 7190−7196.
(54) Pickett, H. M. The Fitting and Prediction of Vibration-Rotation Spectra with Spin Interactions. *J. Mol. Spectrosc.* **1991**, *148*, 371−377.
(55) Pickett, H. M. SPFIT/SPCAT Package, available at http://spec.jpl.nasa.gov.
(56) Cazzoli, G.; Puzzarini, C.; Harding, M. E.; Gauss, J. The Hyperfine Structure in the Rotational Spectrum of Water: Lamb-Dip Technique and Quantum-Chemical Calculations. *Chem. Phys. Lett.* **2009**, *473*, 21−25.
(57) Puzzarini, C.; Cazzoli, G.; Harding, M. E.; Vázquez, J.; Gauss, J. A New Experimental Absolute Nuclear Magnetic Shielding Scale for

Oxygen Based on the Rotational Hyperfine Structure of $H_2{}^{17}O$. *J. Chem. Phys.* **2009**, *131*, 234304/1−11.
(58) Cazzoli, G.; Puzzarini, C.; Stopkowicz, S.; Gauss, J. Hyperfine Structure in the Rotational Spectra of Trans-Formic Acid: Lamb-Dip Measurements and Quantum-Chemical Calculations. *Astron. Astrophys.* **2010**, *520*, A64/1−6.
(59) Puzzarini, C.; Cazzoli, G.; López, J. C.; Alonso, J. L.; Baldacci, A.; Baldan, A.; Stopkowicz, S.; Cheng, L.; Gauss, J. Spectroscopic Investigation of Fluoroiodomethane, CH_2FI: Fourier-Transform Microwave and Millimeter-/Submillimeter-Wave Spectroscopy and Quantum-Chemical Calculations. *J. Chem. Phys.* **2011**, *134*, 174312/1−9.
(60) Kisiel, Z. *PROSPE - Programs for ROtational SPEctroscopy*, available at http://info.ifpan.edu.pl/~kisiel/prospe.htm.